



This open access document is posted as a preprint in the Beilstein Archives at <https://doi.org/10.3762/bxiv.2024.62.v1> and is considered to be an early communication for feedback before peer review. Before citing this document, please check if a final, peer-reviewed version has been published.

This document is not formatted, has not undergone copyediting or typesetting, and may contain errors, unsubstantiated scientific claims or preliminary data.

Preprint Title Hydrogen-bonded macrocycle-mediated dimerization for orthogonal supramolecular polymerization

Authors Wentao Yu, Zhiyao Yang, Chengkan Yu, Xiaowei Li and Lihua Yuan

Publication Date 21 Oct 2024

Article Type Full Research Paper

Supporting Information File 1 Crystal data for H+G1.cif; 63.3 KB

Supporting Information File 2 Supporting Information.pdf; 1.8 MB

ORCID® iDs Wentao Yu - <https://orcid.org/0009-0006-7444-8248>; Zhiyao Yang - <https://orcid.org/0000-0001-7994-356X>; Xiaowei Li - <https://orcid.org/0000-0001-9479-4857>; Lihua Yuan - <https://orcid.org/0000-0003-0578-4214>



License and Terms: This document is copyright 2024 the Author(s); licensee Beilstein-Institut.

This is an open access work under the terms of the Creative Commons Attribution License (<https://creativecommons.org/licenses/by/4.0>). Please note that the reuse, redistribution and reproduction in particular requires that the author(s) and source are credited and that individual graphics may be subject to special legal provisions.

The license is subject to the Beilstein Archives terms and conditions: <https://www.beilstein-archives.org/xiv/terms>.

The definitive version of this work can be found at <https://doi.org/10.3762/bxiv.2024.62.v1>

Hydrogen-bonded macrocycle-mediated dimerization for orthogonal supramolecular polymerization

Wentao Yu, Zhiyao Yang, Chengkan Yu, Xiaowei Li* and Lihua Yuan*

Address:

College of Chemistry, Sichuan University, Chengdu 610064, China

Email: Xiaowei Li* - lixw@scu.edu.cn; Lihua Yuan* - lhyuan@scu.edu.cn

* Corresponding author

Abstract

Orthogonal self-assembly represents a useful methodology to construct supramolecular polymers with AA and AB type monomers as commonly used for covalent bond-linked polymers. So far, the design of such monomers has relied heavily on three-dimensional macrocycles and the use of two-dimensional shape-persistent macrocycle for this purpose remains rather rare. Here, we demonstrate a dimerization motif based on a hydrogen-bonded macrocycle that can be effectively applied to form orthogonal supramolecular polymers. The macrocycle-mediated connectivity was confirmed by single crystal X-ray diffraction, which reveals a unique 2:2 binding motif between host and guest bridged by two cationic pyridinium end groups through π -stacking interactions and other cooperative intermolecular forces. Zinc ion-induced coordination with the macrocycle and a terpyridinium derivative enables orthogonal polymerization as revealed by ^1H NMR, DLS, and TEM techniques. In addition,

viscosity measurements show a transition from oligomers to polymers at the critical polymerization concentration of 17 μM . These polymers are highly concentration dependent. Establishing this new dimerization motif with shape-persistent H-bonded macrocycle widens the scope of options of non-covalent building blocks for supramolecular polymers and augurs well for the future development of functional materials.

Keywords

orthogonal self-assembly; shape-persistent; hydrogen-bonded macrocycle; supramolecular polymer

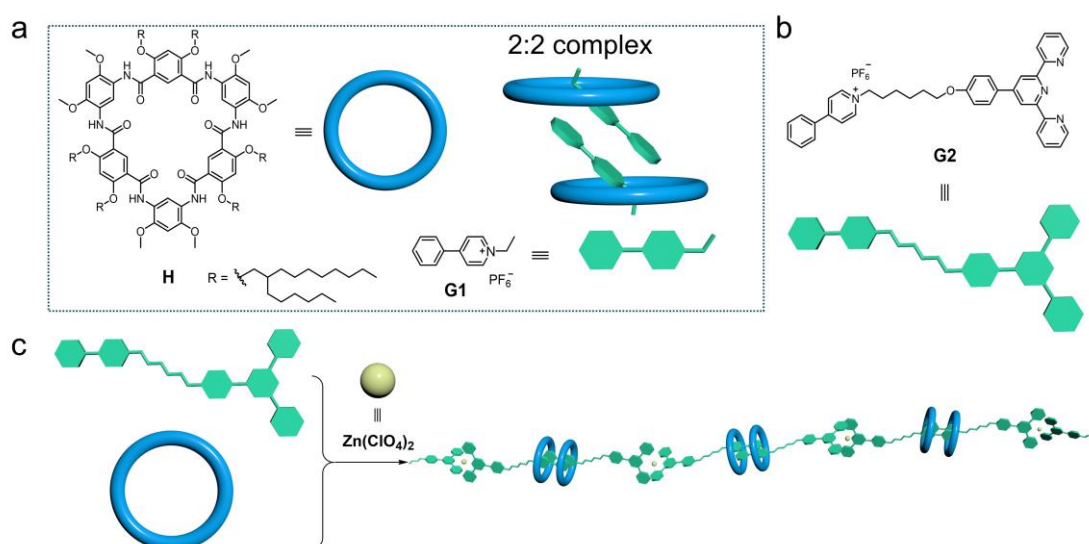
Introduction

Host-guest interactions, particularly those involving macrocycles as host [1] [2], have found a myriad of applications in supramolecular chemistry [3] [4] [5] owing to their ability in creating non-covalent, dynamic, yet strong forces in some cases between molecules. Adding additional element of interactions to supramolecular systems endows them with a feature of “orthogonal self-assembly”, a process in which molecular species are assembled into aggregates by two or more than two types of non-covalent interactions that work independently with respect to each other [6][7]. Generating such motifs with orthogonal propensity is appealing not only in constructing supramolecular polymers with the ability of modulating their structure and properties in multiple ways through adjusting non-covalent bonding interactions, but also conferring supramolecular assemblies with higher complexity and multilevel ordering [8][9][10], leading to a vast number of applications, for example, for use in detection and separation [11], sensing [12], photocatalysis [13], release [14] and as thermochromic

and photoluminescence materials [15]. In this regard, macrocycles emerge a decade ago as a “sticking” end for homo- and hetero-difunctional monomers enabling supramolecular polymerization [16]. So far, macrocycles that are applied to orthogonal self-assembly have been limited to three-dimensional rings such as cucurbituril [17], cyclodextrin [18] and calix[4]pyrrole [19], as well as flexible crown ethers [10][20]. Few two-dimensional (2D) shape-persistent macrocyclic compounds are used for this purpose. One of the difficulties in realizing 2D macrocycle-based orthogonal assembly stems from the requirement for the construction motif, e.g., one end of which should be capable of dimerization by binding to a macrocycle in 2:2 stoichiometry [21][22]. Such binding motifs are intriguing in terms of macrocycle-mediated supramolecular dimerization since they may enable multiple modes of non-covalent connectivity by combining it with other noninterfering interactions (e.g., metal coordination interactions and hydrogen bonding), providing access to constructing varying multi-responsive orthogonal self-assemblies or smart supramolecular polymers [23][24]. For example, the discovery of cucur[8]bituril complexation in 1:2 and 2:2 host-guest stoichiometry leads to a wide spectrum of applications, which include catalysis [25], gelation [26], sensing [27] and color-tuning, etc. [28]. However, only several kinds of macrocycles are capable of implementing supramolecular dimerization through host-guest interactions [29].

Shape-persistent macrocycles have captured interests of chemists for decades [30][31] due to not only their rich host-guest chemistry, but also π -surface-enabled self-assembly capabilities that enable creation of various supramolecular structures such as discotic liquid crystals [32], nano-dimer [33], and organic framework [34]. Among them, shape-persistent hydrogen-bonded aromatic amide macrocycles [35][36][37][38] [39][40][41] a class of cyclic compounds comprising a number of aromatic residues with consecutive intramolecular hydrogen bonds and amide linkages, stand out as a

versatile host molecule, as their cavity size, peripheral side chains, recognition sites are tunable to suit desired functions. These macrocycles have found widespread applications owing to their unique host-guest behaviors in the fields of recognition [42], ion channel [43], catalysis [44], liquid-crystal materials [45], rotaxanes [46] as well as molecular machines [47]. We envisioned that use of a H-bonded aromatic amide macrocycle with six aromatic residues (hereafter called cyclo[6]aramide for brevity, Scheme 1a) can be candidate options as host for mediating dimerization since such a two-dimensional macrocycle has six carbonyl oxygen atoms pointing inwards as binding sites, demonstrating excellent affinity for cationic organic guests including pyridinium and its derivatives [40]. More importantly, it favors intermolecular pi-stacking interactions with aromatic guests [48]. Herein, we report on a novel supramolecular dimerization motif in 2:2 stoichiometry using H-bonded aramide macrocycle for constructing an orthogonal supramolecular polymer (Scheme 1). The terpyridyl group and the pyridinium cation in the AB-type monomer (**G2**) each function as a “sticker” to enable supramolecular polymerization in the presence of the macrocy-



Scheme 1: (a) Chemical structures of H-bonded macrocycle **1a** and guest molecules **G1** and **G2**. (b) Schematic representation of the supramolecular polymer through orthogonal self-assembly upon addition of zinc ions.

clic component and zinc ions. The driving force for the recognition involves multiple cooperative interactions, particularly π -stacking interactions between the aromatic rings in a parallel fashion from both host and guest, which is demonstrated by the crystal structure of the key element of the recognition motif.

Results and Discussion

Backdrop for design consideration

Our interest in macrocycle-mediated supramolecular dimerization is triggered by the observation in mass spectroscopy experiments when exploring host-guest interactions. Positive-ion electrospray ionization mass spectrometry (ESI(+)-MS;

Figure 1) of a

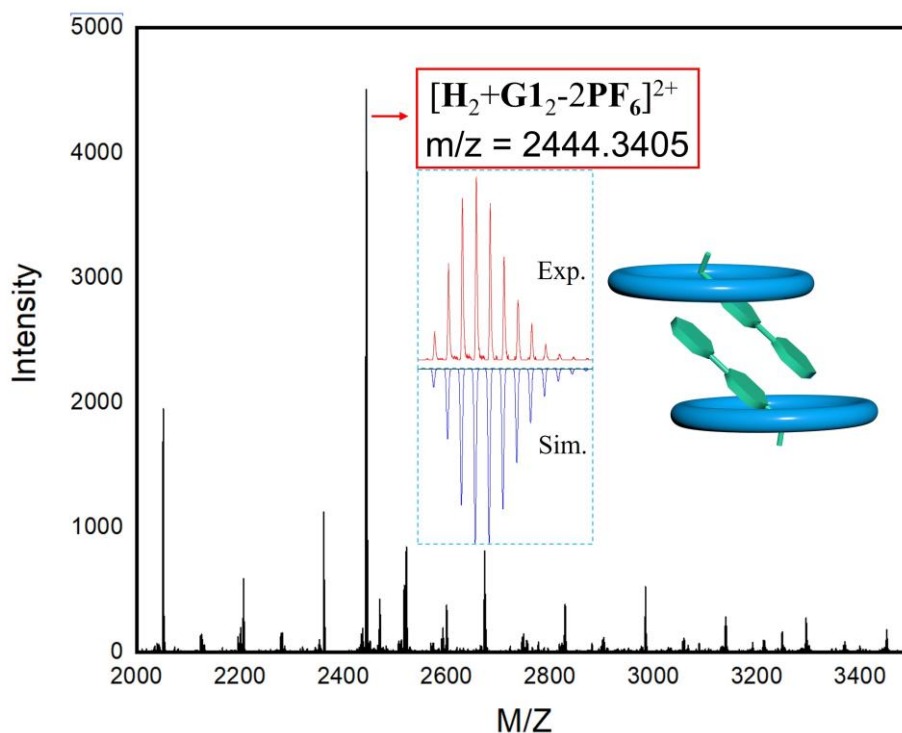


Figure 1: ESI-MS spectrum of an equimolar mixture of **G1** and **H** in CHCl₃/CH₃CN (1:1, v/v). The calculated (blue) and experimental (red) isotopic distribution for [**H**₂ + **G1**₂ - 2PF₆⁻]²⁺, 2444.3373, found 2444.3405.

sample solution of cyclo[6]aramide **H** and a pyridinium derivative **G1** in CHCl₃/CH₃CN (1:1, v/v) shows a dominant peak at m/z = 2444.3405 corresponding to the cation [**H**₂ + **G1**₂ - 2PF₆⁻]²⁺, indicating the presence of a host-guest complex in 2:2 stoichiometry in gas state. Job plot experiments provide a 1:1 stoichiometry (Figure S9), showing consistency with the molar ratio observed in ESI experiments. These inspiring results prompted us to further examine the interaction between host **H** and **G1** by ¹H NMR spectroscopy. Our prior experience with cyclo[6]aramide guarantees its binding to the cationic guest. Indeed, addition of compound **H** to the guest solution results in a pronounced downfield shift ($\Delta\delta = + 0.694$ ppm) of protons H¹ relative to the proton resonance of free guest **G1** in CDCl₃/CD₃CN (1:1, v/v) (Figure 2). Proton H⁶ also

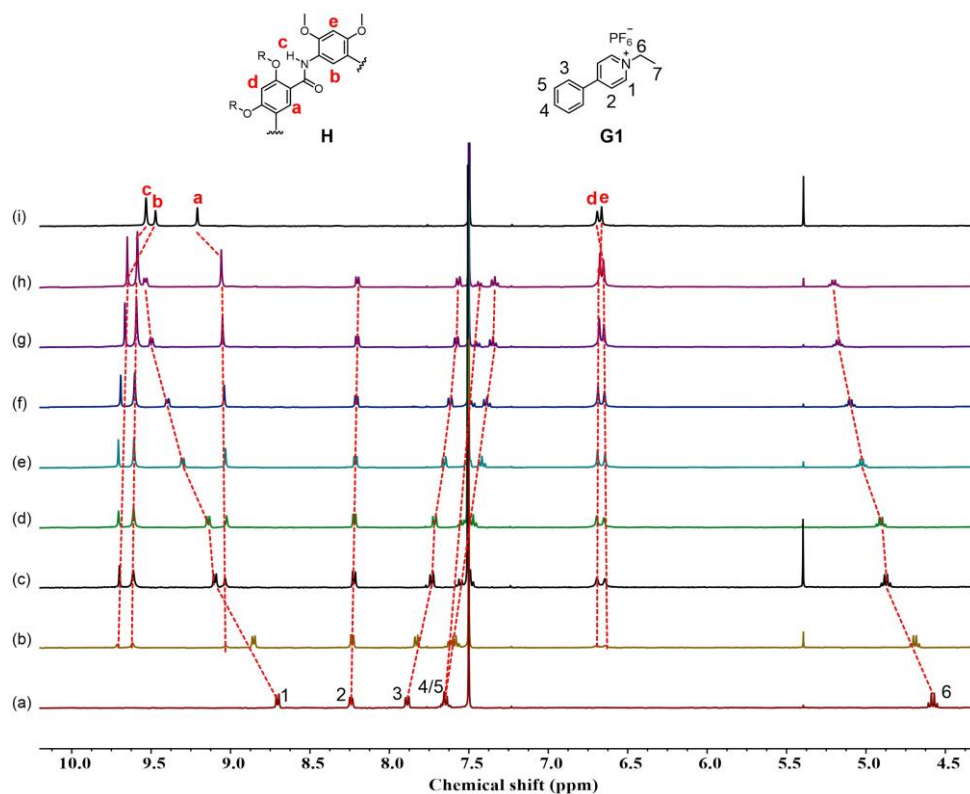


Figure 2: Stacked ^1H NMR spectra ($\text{CDCl}_3/\text{CD}_3\text{CN}$, 1:1, v/v, 400 MHz, 298 K) of **G1** upon addition of different equiv of **H** ($[\text{G1}] = 1.0 \times 10^{-3}$ M, $[\text{H}]/[\text{G1}] = 0 - 1.4$ eq). (a) 0.0 eq, (b) 0.2 eq, (c) 0.4 eq, (d) 0.6 eq, (e) 0.8 eq, (f) 1.0 eq, (g) 1.2 eq, (h) 1.4 eq, and (i) only **H**.

experiences a larger downfield shift ($\Delta\delta = + 0.519$ ppm). The fact that all other resonances for protons $\text{H}^2\text{-H}^5$ only show a relatively smaller lower frequency shifts ($\Delta\delta = -0.033\text{-}0.270$ ppm) with respect to those of protons H^1 and H^6 suggests that the macrocycle tends to reside around the cationic pyridinium site in the binding process. On the other hand, accompanied by the change of chemical shifts for the protons of **G1** is the resonance change of internal aromatic protons H^a and H^b in the host **H** ($\Delta\delta = - 0.170$ ppm, $\Delta\delta = + 0.218$ ppm), all pointing to the existence of strong host-guest interaction in solution.

Then we attempted to grow the single crystal of the complex out of curiosity, wondering if the 2:2 structure is reliable in the solid state. Fortunately, single crystals of the complex $\text{H} \supset \text{G1}$ were obtained by slow evaporation of the mixed solvent of chloroform and acetone (1:1, v/v) into a small amount of methanol, during the course of two weeks. Indeed, analysis of the crystal structure of the complex reveals a strict 2:2 molar ratio (Figure 3), providing convincing evidence for the dimerization process. The complex

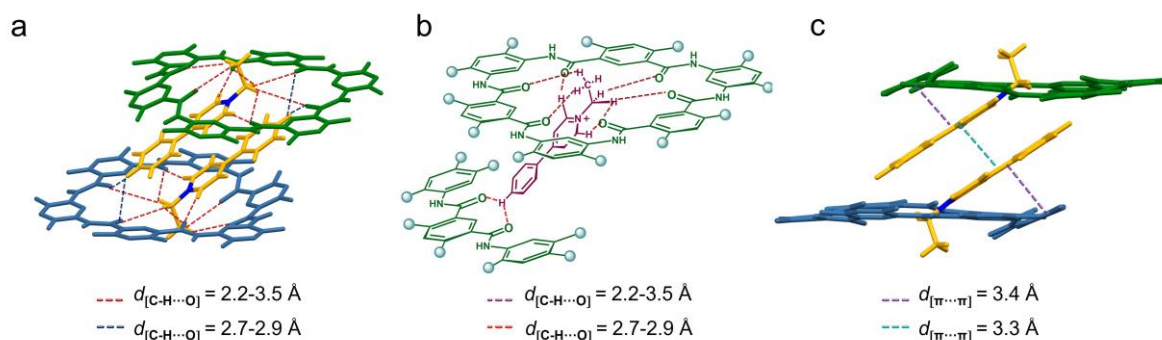


Figure 3: Single-crystal structure of the complex **H** ⊃ **G1**. (a) Dimeric structure formed by cyclo[6]aramide **H** and cationic guest **G1** with each guest molecule threading one molecule of **H** at its end. (b) A portion of the dimeric structure showing an array of hydrogen-bonding interactions between the amide oxygen atoms of **H** and **G1**. The brown dotted line shows the hydrogen bond distance between **H** and the positively charged region of **G1** ($d_{[C-H...O]} = 2.2-3.5 \text{ \AA}$). The red dotted line shows the hydrogen bond distance between **H** and the proton of the phenyl group of **G1** ($d_{[C-H...O]} = 2.7-2.9 \text{ \AA}$). (c) Dimeric structure showing the π - π stacking distances ($d_{[\pi... \pi]} = 3.3-3.4 \text{ \AA}$) between **H** and **G1**.

crystallizes in the triclinic $P\bar{1}$ space group with lattice constants $a = 24.434(4) \text{ \AA}$, $b = 20.026(3) \text{ \AA}$, $c = 23.779(4) \text{ \AA}$. The dimeric superstructure is stabilized by cooperative action of multiple non-covalent interactions, particularly intermolecular π - π stacking and C-H...O interactions. Specifically, π - π stacking interactions are found between two guest molecules with aromatic rings arrayed in an off-set fashion with a distance of 3.3 \AA (Figure 3a). Interestingly, these interactions also exist between one guest and one phenyl ring of the host with a distance of 3.4 \AA . The observation of these short π distances suggests the crucial role of π stacking interactions in sustaining the stability of the 2:2 complex of host **H** and guest **G1**. It is worth mentioning that each of the two macrocycles adopts a non-planar conformation with one aromatic residue protruding out of the macrocyclic skeleton plane. Adopting such conformation renders it possible for the π -electron-rich phenyl ring to interact strongly with π -electron-deficient guest molecules **G1** by means of charge transfer interactions and/or π -stacking interactions, conferring characteristic 2:2 constitutional stoichiometry on this host-guest complex. In addition, there are 8 C-H...O interactions between the hydrogen atoms on **H** and the

nearby pyridinium on **G1** with distances of 2.2-3.5 Å and 2 C-H...O interactions between hydrogen atoms on **G1** and the nearby phenyl groups on **H** with a distance of 2.7-2.9 Å (Figures 3a and 3b). These results above provide conclusive evidence for the 2:2 recognition mode through interaction of two guests with two macrocycles.

With this host-guest complex pattern in 2:2 stoichiometry in mind, a guest molecule **G2** consisting of phenyl pyridinium and a terpyridyl group is designed (Scheme 1b) for use in forming a host-guest complex with cyclo[6]aramide **H**. Compound **G2** was synthesized by refluxing **S2** and 4-phenylpyridine in acetonitrile for 24 h (Scheme S2). It is expected that by applying the design rules commonly known with metallo-supramolecular polymers and macrocycle-mediated dimerization in supramolecular chemistry, we are able to generate supramolecular polymers with this hetero-difunctional monomer with one end comprising two macrocycles and the other end coordinating with metal ions. In such supramolecular polymers, orthogonal host-guest and coordination interactions are responsible for polymerization.

Host-guest complexation and zinc coordination

When forming supramolecular polymers, a AB type monomer, i.e., the guest **G2**, is supposed to interact with the macrocycle **H** and a metal ion through each of two end groups (pyridinium and terpyridyl). As such, host-guest complexation and zinc coordination of the AB type monomer were investigated, respectively.

To begin with, the complex-forming ability of host **H** with **G2** was explored by ¹H NMR spectroscopic titrations in a mixed solvent of CDCl₃ and CD₃CN (1:1). Titration of compound **H** to the guest solution results in constant downfield shifts of protons **1** ($\Delta\delta = + 0.889$ ppm) and **13** ($\Delta\delta = + 0.716$ ppm) on the pyridinium moiety, signifying the complexation of the macrocycle at the cationic recognition site. The change in chemical shifts of protons **12** ($\Delta\delta = - 0.416$ ppm) can be explained by ring translocation along

the guest axle due to dynamics in the binding process, which is often observed in pseudo-rotaxanes (Figure 4) [49]. When the molar ratio of **H/G2** reaches 1:1, the original proton signals of the macrocycle disappear completely. Further addition of the macrocycle brings marginal influence on the new set of signals, suggesting formation of an n:n complex of **H** and **G2**. Job plot experiments afforded a stoichiometry of n:n (Figure S10), purporting the probability of 2:2 complexation in solution. A strong indication of the formation of 2:2 complex comes from ESI-MS experiments. The mass spectra recorded for a mixture comprising **H** and **G2** in 1:1 molar ratio show a multi-charged pseudo-molecular ion peak corresponding to $[\mathbf{H}_2 + \mathbf{G2}_2 + \text{H}^+ - 2\text{PF}_6^-]^{3+}$ and the isotope patterns are in good agreement with theoretical simulations (Figure S12). Therefore, taken together, these experimental results above indicate that the macrocycle **H** has a strong propensity for forming a 2:2 stoichiometric complex with guest **G2**.

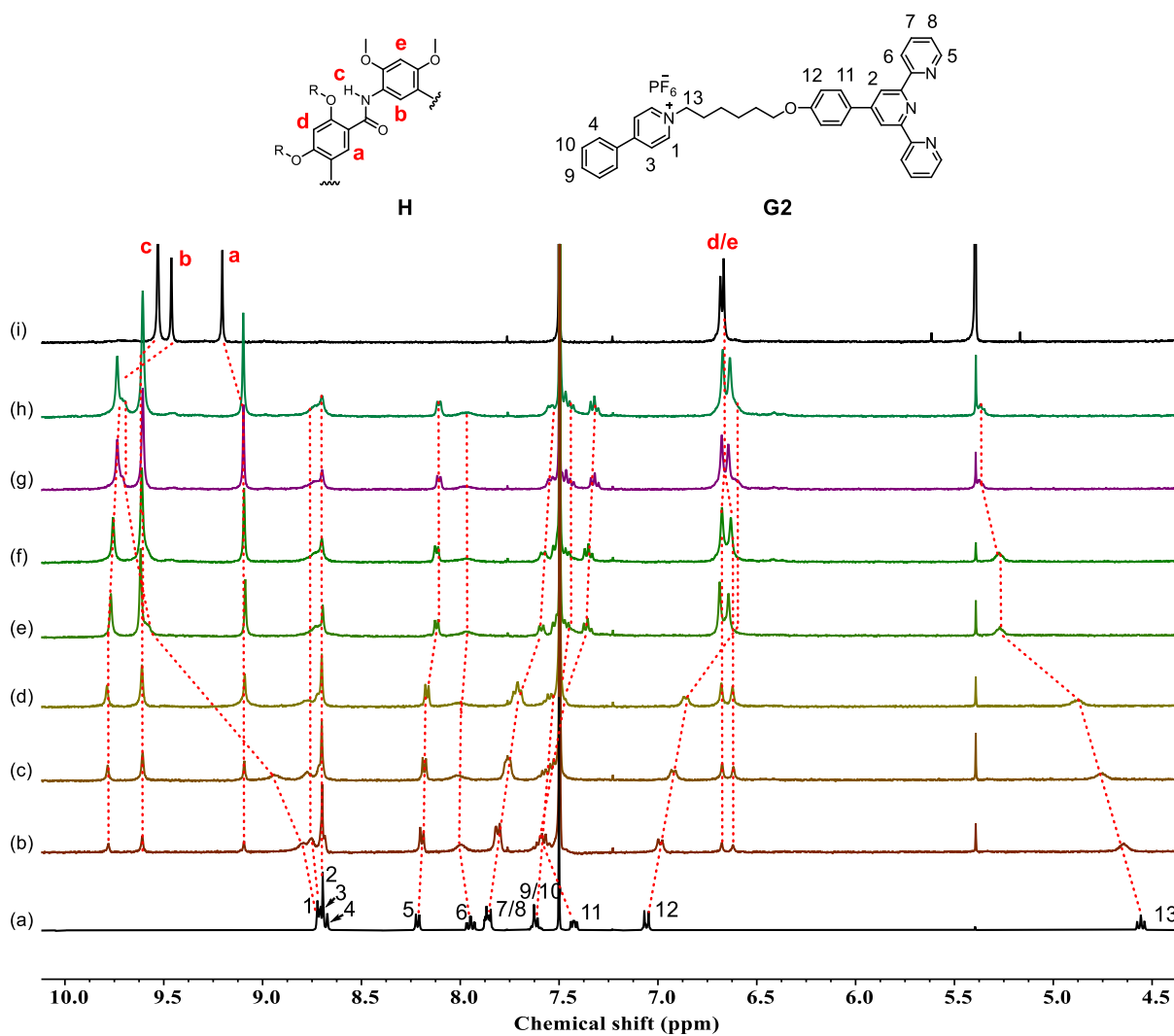


Figure 4: Stacked ¹H NMR spectra (CDCl₃/CD₃CN, 1:1, v/v, 400 MHz, 298 K) of **G2** upon addition of different equiv of **H** ($[\mathbf{G2}] = 1.0 \times 10^{-3}$ M, $[\mathbf{H}]/[\mathbf{G2}] = 0 - 1.4$ eq). (a) 0.0 eq, (b) 0.2 eq, (c) 0.4 eq, (d) 0.6 eq, (e) 0.8 eq, (f) 1.0 eq, (g) 1.2 eq, (h) 1.4 eq, and (i) only **H**.

Examining the ability of coordination with zinc ions constitutes another important aspect of implementing orthogonal self-assembly. To this end, a mixture of **G2** and zinc salt in CHCl₃:CH₃CN (1:1, v/v) was subjected to ¹H NMR spectroscopy. Protons 2, 3, 4, 7, 8, 11 and 12 of **G2** that are located around the metal coordination site were found to experience shifts upfields or downfields to a varying extent (Figure S8). Particularly noteworthy is the pronounced downfield shift ($\Delta\delta = +0.886$ ppm) for the

signal of proton 1. The change in chemical shifts for the protons on the terpyridyl group speak for the coordination of zinc ion with the terpyridyl end.

Orthogonal self-assembly and supramolecular polymerization

The structure feature of **G2** with one end interacting only with macrocycles and the other end coordinating only with metal ions dictates that self-assembly will occur upon addition of either macrocycle or metal ions, but it's unlikely to induce supramolecular polymerization unless both of them are present—a propensity of orthogonal self-assembly. Indeed, when **G2** and zinc salt in 1:1 molar ratio are mixed together, results from dynamic light scattering (DLS) experiments show that the average hydrodynamic diameter (D_h) falls in a size distribution of 524 nm, and no particles of discernible size are observed for a mixture of the macrocycle **H** and **G2** or **H** and the salt, whereas with a solution containing **G2**, **H** and zinc salt, the D_h of the aggregates is abruptly increased to 2580 nm (Figure S13). These results strongly indicate that polymerization proceeds only when both macrocycle and metal ion are present. TEM images of **H** + **G2** + Zn^{2+} solution with a respective concentration of 1 mM and 3 mM reveal a nano-globular suprastructure but present a larger nano-irregular block suprastructure at higher concentration (5 mM) (Figure 5).

To support the aggregation formation, 1H NMR titration experiments were carried out by adding the macrocycle **H** in different equivalents to a solution containing a mixture

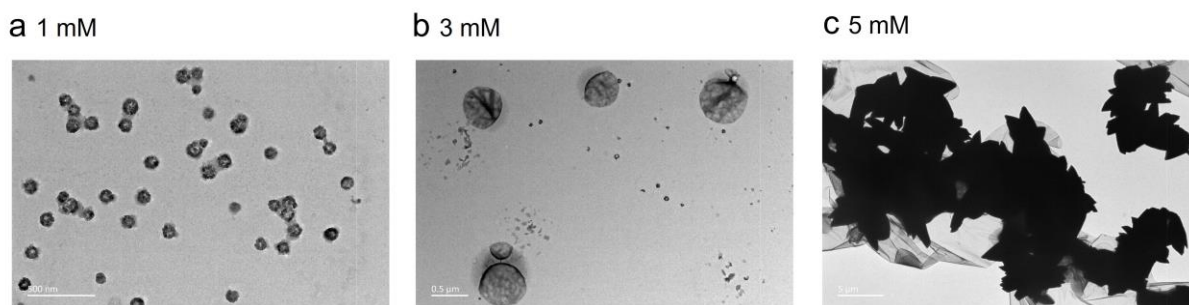


Figure 5: TEM images of **H** + **G2** + Zn(ClO₄)₂ at different concentrations (CHCl₃/CH₃CN = 1:1, v/v, 298 K).

of **G2** and zinc salt in 1:1 molar ratio. Aromatic protons *a* ($\Delta\delta = -0.142$ ppm) and *b* ($\Delta\delta = +0.357$ ppm) are downfield shifted to a great extent, accompanied by the broadening of signals from **G2** (Figure 6). Constant downfield shifts were observed for protons *1* ($\Delta\delta = +0.332$ ppm) and *13* ($\Delta\delta = +0.473$ ppm), protons *10* ($\Delta\delta = -0.397$ ppm) and *12*

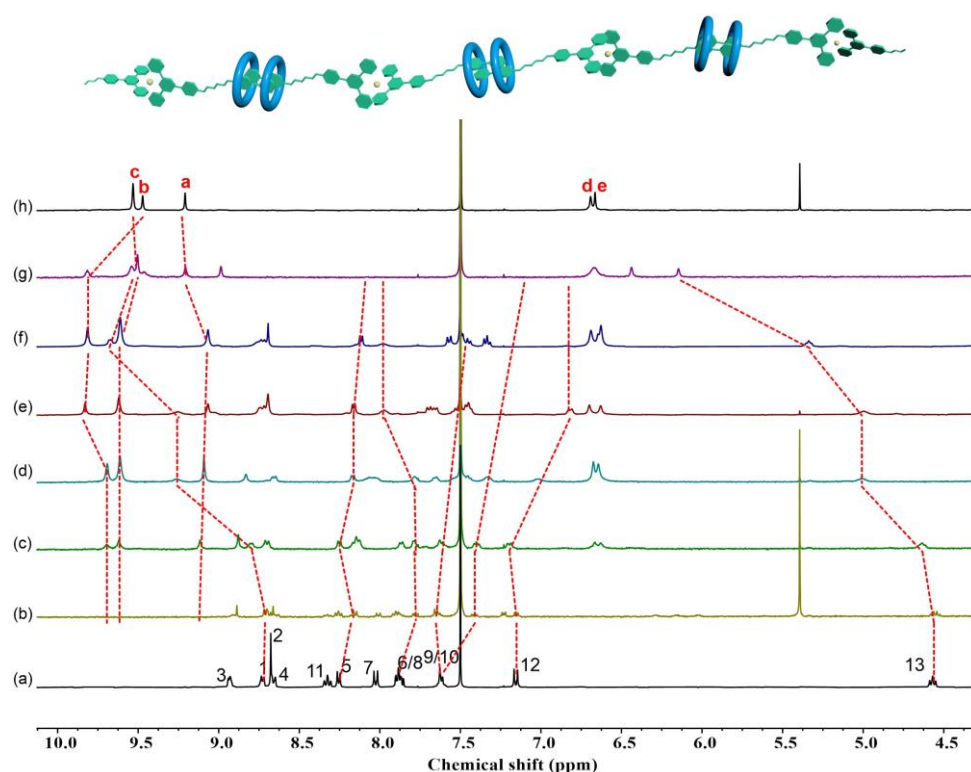


Figure 6: Stacked ¹H NMR spectra (CDCl₃/CD₃CN, 1:1, v/v, 400 MHz, 298 K) of **G2** + Zn²⁺ upon addition of different equiv of **H** (**[G2 + Zn²⁺]** = 1.0 × 10⁻³ M, **[H]/[G2 + Zn²⁺]** = 0 – 1.4 eq). (a) 0.0 eq, (b) 0.4 eq, (c) 0.6 eq, (d) 0.8 eq, (e) 1.0 eq, (f) 1.2 eq, (g) 1.4 eq and (h) only **H**.

($\Delta\delta = +0.246$ ppm) on the pyridinium moiety, signifying the complexation of the macrocycle at the cationic recognition site. The changes in chemical shifts and the broadening of signals before and after addition of the macrocycle to a **G2**:Zn²⁺ complex are consistent with the formation of supramolecular polymers.

The supramolecular polymers formed were further characterized by viscosity and variable-concentration NMR experiments. One important feature of supramolecular polymers is its dependency of its molecular weight on solution concentration, and change in solution viscosity would reflect the change of molecular weight in the polymerization process that occurs between these components including **H**, **G2** and metal ions. Thus, specific viscosities of the linear supramolecular polymer (Scheme 1c) were determined in $\text{CHCl}_3:\text{CH}_3\text{CN}$ (1:1, v:v) at 298 K (Figure 7). The plot of specific viscosity versus concentration shows a changing process in two stages: before the turning point at 17 μM and beyond. The first stage offers a slope of 1.1, corresponding to the formation of oligomeric assemblies in solution. On continuously increasing the concentration beyond 17 μM , a second stage starts and ends up with a slope of 3.4, which is usually considered as an indication of forming linear supramolecular polymers

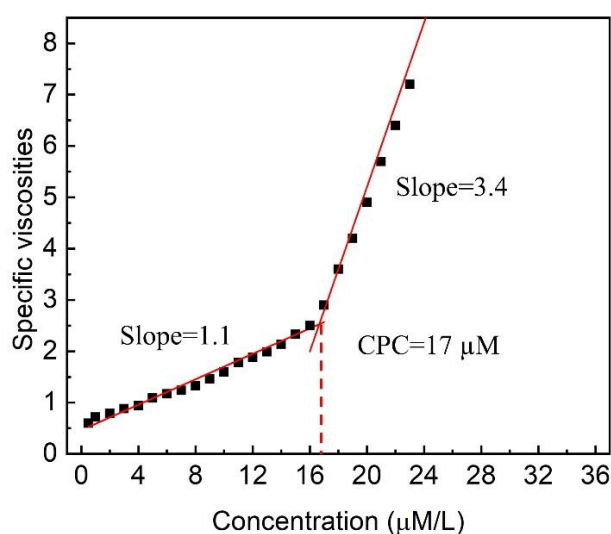


Figure 7: Specific viscosities of the linear supramolecular polymer in $\text{CHCl}_3/\text{CH}_3\text{CN}$ (1:1, v:v, 298 K) at variable concentration.

[50]. The observation of the turning point concentration, or a critical polymerization concentration (CPC) [51] [52], indicates concentration-driven polymerization that is characteristic of formation of supramolecular polymers. The concentration-dependency of a mixture of **H**, **G2** and zinc slat was examined by variable

concentration NMR spectroscopy. Pronounced broadening of signals were observed (Figure 8), which clearly indicates the increased polymerization with raising the concentration of each component.

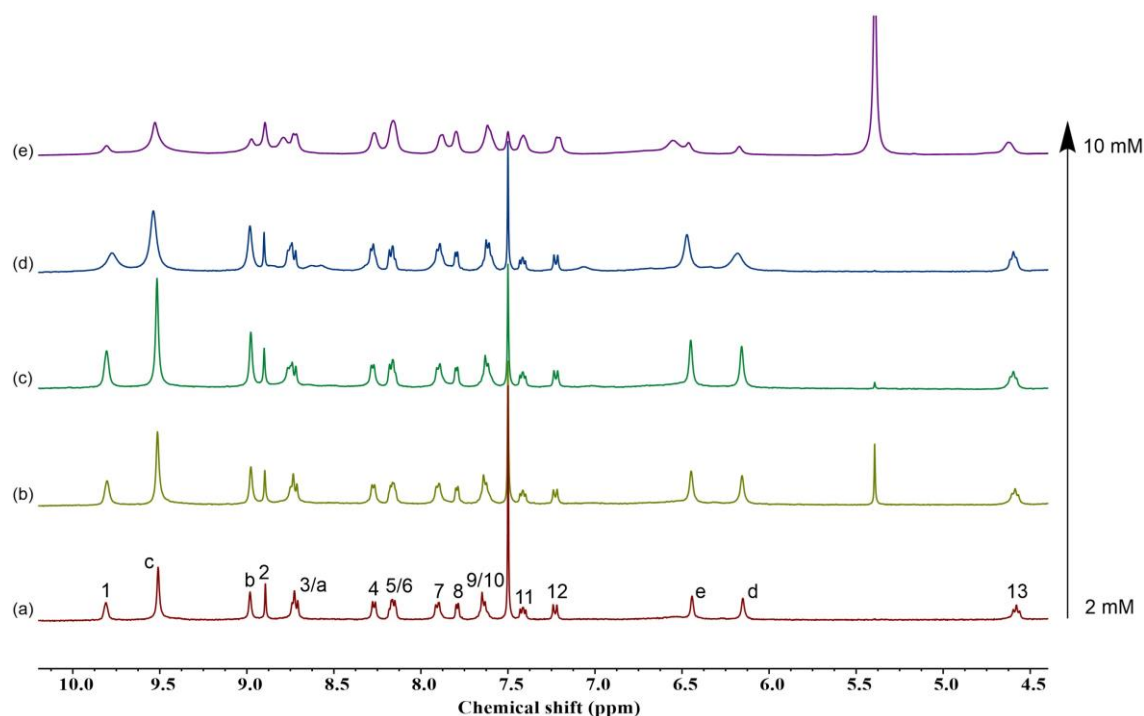


Figure 8: Variable concentration ^1H NMR spectra of the supramolecular polymer: (a) 2.0 mM; (b) 4.0 mM; (c) 6.0 mM; (d) 8.0 mM; (e) 10 mM.

Conclusion

We have described a new recognition motif based on a hydrogen-bonded amide macrocycle that is used to drive the linear polymerization of a hetero-difunctional monomer in the presence of zinc ions. Apart from the role of hydrogen-bonding interactions, the 2:2 host-guest dimerization is enabled owing largely to a result of an increased accessibility for π -stacking interactions between two guests themselves and between guest and the macrocycle. Such 2:2 connectivity mode makes shape-persistent H-bonded macrocycle useful macrocyclic component for creating orthogonal

supramolecular polymers and bodes well for future use in designing stimuli-responsive and smart polymers.

Supporting Information

Supporting Information File 1

Experimental and copies of spectra.

Supporting Information File 2

Crystallographic data of **H** \supset **G1** analysed by SHELX (CCDC 2384953).

Acknowledgements

We thank Dr Dongyan Deng from the College of Chemistry, Dr Pengchi Deng and Dr Chen Yuan from The Analytical & Testing Center, Sichuan University for analytic testing and valuable help.

Funding

This research was financially supported by the National Natural Science Foundation of China (22271202 to L. Y., 22201193 to X. L.), the Sichuan Science and Technology Program (2023NSFSC0109 to X. L.), the Fundamental Research Funds for the Central Universities and the Hundred Talent Program of Sichuan University (YJ2021158 to X. L.), Open Project of State Key Laboratory of Supramolecular Structure and Materials (SKLSSM2024037).

ORCID® iDs

Wentao Yu - <https://orcid.org/0009-0006-7444-8248>

Zhiyao Yang - <https://orcid.org/0000-0001-7994-356X>

Xiaowei Li - <https://orcid.org/0000-0001-9479-4857>

Lihua Yuan - <https://orcid.org/0000-0003-0578-4214>

Data Availability Statement

All data that supports the findings of this study is available in the published article and/or the supporting information to this article. The crystallographic data were deposited in the Cambridge Crystallographic Data Centre (CCDC 2384953). The data can be obtained free of charge from the CCDC via http://www.ccdc.cam.ac.uk/data_request/cif.

References

1. Ji, X.; Ahmed, M.; Long, L.; Khashab, N. M.; Huang, F.; Sessler, J. L. *Chem. Soc. Rev.*, **2019**, *48*, 2682–2697.
2. Xia, D.; Wang, P.; Ji, X.; Khashab, N. M.; Sessler, J. L.; Huang, F. *Chem. Rev.*, **2020**, *120*, 6070–6123.
3. Yang, H.; Yuan, B.; Zhang, X.; Scherman, O. A. *Acc. Chem. Res.*, **2014**, *47*, 2106–2115.
4. Yan, M.; Wu, S.; Wang, Y.; Liang, M.; Wang, M.; Hu, W.; Yu, G.; Mao, Z.; Huang, F.; Zhou, J. *Adv. Mater.*, **2024**, *36*, 2304249.
5. Yu, G.; Jie, K.; Huang, F. *Chem. Rev.*, **2015**, *115*, 7240–7303.
6. Huck, W. T.; Hulst, R.; Timmerman, P.; van Veggel, F. C.; Reinhoudt, D. N. *Angew. Chem. Int. Ed.*, **1997**, *36*, 1006–1008.
7. Wong, C.-H.; Zimmerman, S. C. *Chem. Commun.*, **2013**, *49*, 1679–1695.

-
8. Wei, P.; Yan, X.; Huang, F. *Chem. Soc. Rev.*, **2015**, *44*, 815–832.
 9. Xiao, T.; Zhou, L.; Sun, X.-Q.; Huang, F.; Lin, C.; Wang, L. *Chin. Chem. Lett.*, **2020**, *31*, 1-9.
 10. Hu, X.-Y.; Xiao, T.; Lin, C.; Huang, F.; Wang, L. *Acc. Che. Res.*, **2014**, *47*, 2041–2051.
 11. Li, Y.; Lou, X.; Wang, C.; Wang, Y.; Jia, Y.; Lin, Q.; Yang, Y. *Chin. Chem. Lett.*, **2023**, *34*, 107877.
 12. Xu, L.; Chen, D.; Zhang, Q.; He, T.; Lu, C.; Shen, X.; Tang, D.; Qiu, H.; Zhang, M.; Yin, S. *Polym. Chem.*, **2018**, *9*, 399-403.
 13. Bai, Z.; Velmurugan, K.; Tian, X.; Zuo, M.; Wang, K.; Hu, X.-Y., *Beilstein J. Org. Chem.* **2022**, *18*, 429-437.
 14. Samanta, S. K.; Quigley, J.; Vinciguerra, B.; Briken, V.; Isaacs, L. *J. Am. Chem. Soc.*, **2017**, *139*, 9066–9074.
 15. Wu, H.; Chen, Y.; Dai, X.; Li, P.; Stoddart, J. F.; Liu, Y. *J. Am. Chem. Soc.*, **2019**, *141*, 6583–6591.
 16. Yang, L.; Tan, X.; Wang, Z.; Zhang, X. *Chem. Rev.*, **2015**, *115*, 7196-7239.
 17. Barrow, S. J.; Kasera, S.; Rowland, M. J.; Del Barrio, J.; Scherman, O. A. *Chem. Rev.*, **2015**, *115*, 12320–12406.
 18. Xia, Z.; Song, Y.-F.; Shi, S. *Angew. Chem. Int. Ed.*, **2024**, *63*, e202312187.
 19. Budak, A.; Aydogan, A. *Chem. Commun.*, **2021**, *57*, 4186-4189.
 20. Wei, P.; Yan, X.; Cook, T. R.; Ji, X.; Stang, P. J.; Huang, F. *ACS. Macro. Lett.*, **2016**, *5*, 671-675.
 21. Chen, Y.; Kuvayskaya, A.; Pink, M.; Sellinger, A.; Flood, A. H. *Chem. Sci.*, **2024**, *15*, 389-398.

-
22. Zhao, W.; Qiao, B.; Tropp, J.; Pink, M.; Azoulay, J. D.; Flood, A. H. *J. Am. Chem. Soc.*, **2019**, *141*, 4980-4989.
 23. Yu, H.-J.; Zhou, X.-L.; Dai, X.; Shen, F.-F.; Zhou, Q.; Zhang, Y.-M.; Xu, X.; Liu, Y. *Chem. Sci.*, **2022**, *13*, 8187-8192.
 24. Olesińska, M.; Wu, G.; Gómez-Coca, S.; Antón-García, D.; Szabó, I.; Rosta, E.; Scherman, O. A. *Chem. Sci.*, **2019**, *10*, 8806-8811.
 25. Tang, B.; Xu, W.; Xu, J.-F.; Zhang, X. *Angew. Chem. Int. Ed.*, **2021**, *60*, 9384-9388.
 26. Yang, X.; Wang, R.; Kermagoret, A.; Bardelang, D. *Angew. Chem. Int. Ed.*, **2020**, *59*, 21280-21292.
 27. Zhang, X.-D.; Fang, F.; Chen, K.; Ni, Y. *Dyes and Pigments.*, **2024**, *227*, 112181.
 28. Xia, D.; Wang, P.; Ji, X.; Khashab, N. M.; Sessler, J. L.; Huang, F. *Chem. Rev.*, **2020**, *120*, 6070-6123.
 29. Zha Wu, G.; Li, F.; Tang, B.; Zhang, X. *J. Am. Chem. Soc.*, **2022**, *144*, 14962-14975.
 30. Zhang, W.; Moore, J. S. *Angew. Chem. Int. Ed.*, **2006**, *45*, 4416-4439.
 31. Höger, S. *Chem. Eur. J.*, **2004**, *10*, 1320-1329.
 32. Li, X.; Li, B.; Chen, L.; Hu, J.; Wen, C.; Zheng, Q.; Wu, L.; Zeng, H.; Gong, B.; Yuan, L. *Angew. Chem. Int. Ed.*, **2015**, *54*, 11147-11152.
 33. Klyatskaya, S.; Dingenouts, N.; Rosenauer, C.; Müller, B.; Höger, S. *J. Am. Chem. Soc.*, **2006**, *128*, 3150-3151.
 34. Gomez, E.; di Nunzio, M. R.; Moreno, M.; Hisaki, I.; Douhal, A. *J. Phys. Chem. C.*, **2020**, *124*, 6938-6951.
 35. Gong, B.; Shao, Z. *Acc. Chem. Res.* **2013**, *46*, 2856-2866.
 36. Ong, W.; Zeng, H. *J. Inclusion Phenom. Mol. Recognit. Chem.*, **2013**, *76*, 1-11.
 37. Zhang, D.; Zhao, X.; Hou, J.; Li, Z. *Chem. Rev.*, **2012**, *112*, 5271-5316.

-
38. Liu, Z.; Zhou, Y.; Yuan, L. *Org. Biomol. Chem.*, **2022**, *76*, 1–11.
39. Huang, S.; Li, X.; Cai, Y.; Feng, W.; Yuan, L. *Chem. Eur. J.*, **2024**, *30*, e202303394.
40. Lu, K.; Zhang, P.; Yue, Y.; Yuan, X.; Yuan, L.; Feng. *PRZEM. CHEM.*, **2017**, *96*, 1906-1912.
41. Zhu, Y.; Chen, C.; Sangaraiah, N.; Kannekanti, V. K.; Yuan, L.; Feng, W. *J. Iran. Chem. Soc.*, **2018**, *15*, 2861-2869.
42. Ren, C.; Shen, J.; Zeng, H. *Org. Lett.*, **2015**, *17*, 5946–5949.
43. Helsel, A.; Brown, A.; Yamato, K.; Feng, W.; Yuan, L.; Clements, A.; Harding, S.; Szabo, G.; Shao, Z.; Gong, B. *J. Am. Chem. Soc.*, **2008**, *130*, 15784–15785.
44. Kang, K.; Lohrman, J.; Nagarajan, S.; Chen, L.; Deng, P.; Shen, X.; Fu, K.; Feng, W.; Johnson, D.; Yuan, L. *Org. Lett.*, **2019**, *21*, 652–655.
45. Li, X.; Li, B.; Chen, L.; Hu, J.; Wen, C.; Zheng, Q.; Wu, L.; Zeng, H.; Gong, B.; Yuan, L. *Angew. Chem. Int. Ed.*, **2015**, *54*, 11147–11152.
46. Huang, S.; Wang, Z.; Wu, J.; Mai, X.; Qin, S.; Zhou, Y.; Yuan, D.; Li, X.; Feng, W.; Yuan, L. *Chem. Commun.*, **2024**, *60*, 5622-5625.
47. Yang, Z.; Wang, X.; Penocchio, E.; Ragazzon, G.; Chen, X.; Lu, S.; Zhou, Y.; Fu, K.; Liu, Z.; Cai, Y.; Yu, X.; Li, X.; Li, X.; Feng, W.; Yuan, L. *Angew. Chem. Int. Ed.* e202414072.
48. Xu, M.; Chen, L.; Jia, Y.; Mao, L.; Feng, W.; Ren, Y.; Yuan, L. *Supramol. Chem.*, **2015**, *27*, 436-443.
49. Wang, Q.; Zhang, P.; Li, Y.; Tian, L.; Cheng, M.; Lu, F.; Lu, X.; Fan, Q.; Huang, W. *RSC. Adv.*, **2017**, *7*, 29364-29367.
50. Wu, L.; Han, C.; Wu, X.; Wang, L.; Caochen, Y.; Jing, X. *Dalton. Trans.*, **2015**, *44*, 20334-20337.

51. Scherman, O. A.; Ligthart, G. B. W.; Sijbesma, R. P.; Meijer, E.W. *Angew. Chem. Int. Ed.*, **2006**, *45*, 2072.

52. Liu, Y.; Wang, Z.; Zhang, X. *Chem. Soc. Rev.*, **2012**, *41*, 5922.